JOURNAL OF NEUROTRAUMA 34:220–234 (January 1, 2017)

DOI: 10.1089/neu.2015.4372

Traumatic Brain Injury Induces Alterations in Cortical Glutamate Uptake without a Reduction in Glutamate Transporter-1 Protein Expression

Christopher R. Dorsett,[1,*] Jennifer L. McGuire,[2,*] Tracy L. Niedzielko,[3] Erica A.K. DePasquale,[2] Jaroslaw Meller,[4,5] Candace L. Floyd,[3] and Robert E. McCullumsmith[2]

Abstract

We hypothesize that the primary mechanism for removal of glutamate from the extracellular space is altered after traumatic brain injury (TBI). To evaluate this hypothesis, we initiated TBI in adult male rats using a 2.0 atm lateral fluid percussion injury (LFPI) model. In the ipsilateral cortex and hippocampus, we found no differences in expression of the primary glutamate transporter in the brain (GLT-1) 24 h after TBI. In contrast, we found a decrease in glutamate uptake in the cortex, but not the hippocampus, 24 h after injury. Because glutamate uptake is potently regulated by protein kinases, we assessed global serine-threonine protein kinase activity using a kinome array platform. Twenty-five kinome array peptide substrates were differentially phoshorylated between LFPI and controls in the cortex, whereas 19 peptide substrates were differentially phosphorylated in the hippocampus (fold change $\geq \pm 1.15$). We identified several kinases as likely to be involved in acute TBI, including protein kinase B (Akt) and protein kinase C (PKC), which are well-characterized modulators of GLT-1. Exploratory studies using an inhibitor of Akt suggest selective activation of kinases in LFPI versus controls. Ingenuity pathway analyses of implicated kinases from our network model found apoptosis and cell death pathways as top functions in acute LFPI. Taken together, our data suggest diminished activity of glutamate transporters in the prefrontal cortex, with no changes in protein expression of the primary glutamate transporter GLT-1, and global alterations in signaling networks that include serine-threonine kinases that are known modulators of glutamate transport activity.

Keywords: astrocyte; GLT-1; glutamate; kinome array; membrane vesicles

Introduction

Traumatic brain injury (TBI) is a persistent major health problem in the United States, with an annual incidence rate of ~200 per 100,000 people and ~10,000,000 hospitalizations or deaths per year.[1] TBI can lead to long-lasting cognitive and behavioral impairments, and is the leading cause of death resulting from injury in individuals <45 years of age.[2] Although the trauma itself is typically a one-time event, TBI can be understood as an ongoing pathological process consisting of two distinct phases. The initial stage, primary injury, is a direct result of the mechanical forces applied to the brain that induce hemorrhage, contusion, and axonal shearing. The second stage, secondary injury, is characterized as a prolonged, diffuse pathophysiological sequence of events, which may include release of excitatory neurotransmitters, free radical production, mitochondrial damage, changes in protein expression, and cell death.[3]

The metabolic and cellular derangements that are characteristic of the secondary injury phase are largely initiated by massive and indiscriminant release of glutamate into the extracellular space.[4] Although glutamate is the primary excitatory neurotransmitter in the mammalian central nervous system, its interstitial concentrations must be actively maintained, as it can be toxic to neurons even at low extracellular concentrations.[5] Various microdialysis studies demonstrate that within minutes of a person's sustaining a TBI, extracellular glutamate levels rise sharply in a force-dependent

[1]Biological and Biomedical Sciences Doctoral Program, University of North Carolina at Chapel Hill, Chapel Hill, North Carolina.
[2]Department of Psychiatry and Behavioral Neuroscience, University of Cincinnati, Cincinnati, Ohio.
[3]Department of Physical Medicine and Rehabilitation, University of Alabama at Birmingham, Birmingham, Alabama.
[4]Departments of Environmental Health, Electrical Engineering & Computing Systems, and Biomedical Informatics, University of Cincinnati College of Medicine, Cincinnati, Ohio.
[5]Department of Biomedical Informatics, Cincinnati Children's Hospital Medical Center, Cincinnati, Ohio.
*The first two authors contributed equally.

manner,[6] with some reports indicating a ninefold increase in extracellular glutamate levels following a severe lateral fluid percussion injury (LFPI).[7] These excitotoxic levels of extracellular glutamate arise from a number of factors. The mechanical force associated with the primary injury can result in direct disruption of the cell's plasma membrane and lead to indiscriminate electrical discharge, either of which may precipitate the release of intracellular ions and glutamate into the extracellular space.[4,8] The ionic imbalance and widespread cellular derangement associated with the secondary injury phase may result in astrocyte cell death, caspase-mediated degradation of glutamate transporters, changes in key intracellular signaling pathways, and reversal of sodium-dependent glutamate transport; all of which have been implicated in furthering the pathological sequelae associated with TBI.[8–11]

Extracellular concentrations of glutamate are maintained by a family of sodium- dependent glutamate transporters, which are selectively expressed throughout the mammalian brain on both neurons and glia.[12] The glutamate and aspartate transporter (GLAST) and the glutamate transporter-1 (GLT-1) are expressed primarily in astrocytes, whereas the remaining transporters reside primarily on neurons.[13] Of the astrocyte transporters, GLT-1 is responsible for $\sim$90% of the clearance of glutamate from the synapse in most brain regions.[14] The astrocytic glutamate transporters are crucial for the proper maintenance of extracellular glutamate levels, and alterations in glutamate transporter expression leads to abnormalities of neuronal function and viability.[15–19]

Glutamate transporter function may be compromised following TBI. [20] For example, following controlled cortical impact (CCI)-induced TBI, mRNA and protein levels of GLT-1 were reduced in the rat frontal cortex at 24 and 72 h following the injury.[19] In the LFPI model, GLT-1 protein levels were decreased in the ipsilateral cortex at 7 days post-injury.[21] These findings prompted us to examine the effects of TBI on glutamate transporter expression and activity following acute TBI. We used Western blot analysis, biochemical fractionation, ^{3}H-glutamate uptake assays, and kinome array profiling to investigate glutamate transporter fidelity in a well-characterized model of TBI.

Methods

Animals

Adult male Sprague–Dawley rats (348 ± 40 g, age 8–9 weeks, at time of surgery; Charles River Laboratories International, Inc.) were housed two per cage on a 12 h light/dark cycle in a temperature- (22°C) and humidity-controlled facility and allowed standard rat chow and water *ad libitum*. All animal care and experimental procedure complied with National Institutes of Health (NIH) guidelines and were approved by the Institutional Animal Care and Use Committee of the University of Alabama at Birmingham. For generation of tissue, animals were divided into two groups. Uninjured control animals received trepanation only (Sham, $n=5$), whereas the injured animals received TBI using an LFPI model as described subsequently (TBI, $n=5$). For selected experimental procedures, tissue was also taken from uninjured, non-surgery rats (Naïve, $n=5$). Five animals from each condition were humanely euthanized at 24 h post-treatment, and tissue was processed for isolation of membrane vesicles, electron microscopy (EM), Western blot analysis, and kinome array analysis.

Surgical procedure

Surgical procedure was performed as previously described.[22,23] Briefly, animals were anesthetized with 4% isoflurane gas in an O_2 carrier for 4 min, followed by intraperitoneal injection of 100/10 mg/kg mixture of ketamine/xylazine; anesthesia was maintained via ventilation with 1.5–3% isoflurane gas for the duration of surgery. Normothermia was maintained throughout surgery by keeping the animals on a water-jacketed heating pad. After securing the animal in a stereotaxic frame, a midline scalp incision was made and the skin and fascia reflected to expose the bregma, lambda, and sagittal sutures, as well as the lateral ridge. A 4.8 mm craniectomy was trepanned over the right parietal cortex, midway between bregma and lambda, tangential to the sagittal suture. A rigid plastic injury tube (modified female Luer-lock 20G needle hub) was bonded to the skull with cyanoacrylate adhesive over the open craniectomy with the dura intact, and a stabilizing screw was placed in a burr hole drilled rostral to bregma on the ipsilateral side. The injury tube and stabilizing screw were secured with dental acrylic. The scalp was then sutured and the animal was placed in a warmed recovery cage.

Induction of LFPI

Experimental TBI was performed using a fluid percussive device (VCU Biomedical Engineering, Richmond, VA) as previously described.[22,23] The device consists of a Plexiglas cylinder (60 cm in length and 4.5 cm in diameter) filled with sterile water. A piston is mounted on O-rings at one end and an extracranial pressure transducer (Entran Devices, Inc.) 5 mm tube (internal diameter 2.6 mm) ending in a male Luer-lock is fitted at the other end. The animal was anesthetized with 4% isoflurane gas for 4 min, and TBI (2 atm) was induced by rapidly injecting a small volume of sterile saline into the closed cranial cavity over the right ipsilateral hemisphere with the fluid percussion device. Immediately after the impact, the animal was removed from the device, monitored for duration of apnea and unconsciousness, and re-sutured while receiving supplemental oxygen ventilation. The magnitude of the pressure pulse was measured by a pressure transducer, stored on an oscilloscope, and later converted to atmospheres (atm). The pressure pulse was monitored and controlled in order to deliver an equivalent impact of 2.0 atm to each animal.

Brains were extracted and dissected as previously described, with gross anatomical markers used to divide tissue into 20 separate areas of interest, and immediately flash frozen on dry ice.[24] Tissue was kept at −80°C until needed.

Isolation of membrane vesicles

The membrane vesicle isolation protocol was adapted from previous studies utilizing human cortical tissue and optimized to yield both neuronal and glial membrane elements.[25] Frozen cortical tissue (150–200 mg) from the area of injury or the ipsilateral hippocampus (HPC) was transferred to 5 mL of ice-cold HEPES-buffered sucrose solution (HBSS) at pH 7.4 in a glass homogenizer (Kontes Glass Co, #21, Vineland, NJ) and dounced (15 strokes). The homogenate was transferred to microcentrifuge tubes and spun at 800*g* (3000 rpm) for 10 min at 4°C. The supernatant was transferred to new microcentrifuge tubes and spun at 10,000*g* for 15 min at 4°C. The resulting pellet was resuspended in 2 mL of HBSS and layered onto 3 mL of 1.2 M sucrose in a swinging bucket rotor (Beckman Coulter, SW60Ti, Pasadena, CA) and spun at 230,000*g*, 45 min at 4°C. The band above the sucrose gradient (supernatant) was collected and placed in 1.5 mL of either standard glutamate uptake buffer (NaCl, 144 mM; KCl, 2.5 mM; CaCl2, 1.2 mM; MgCl2, 1.2 mM; K2HPO4, 1.3 mM; glucose, 10mM; HEPES, 10 mM; and Tris, 5 mM), or a sodium-free glutamate uptake buffer with choline chloride (144 mM) substituted for sodium chloride. The supernatant was then pipetted onto a 2.5 mL column of 0.8 M sucrose and spun at 230,*000g*, 45 min at 4°C. The pellet was collected and suspended in 100 μL of glutamate uptake buffer with or without sodium. Total protein concentration was determined for each sample with a bicinchoninic acid (BCA) assay.

[^{3}H]-glutamate uptake

Sample tubes were prepared with 20 μg of re-suspended synaptosomes, and placed into tubes containing either standard glutamate uptake buffer at 37°C (37°, $n=5$), standard glutamate uptake buffer at 0°C (0°, $n=5$), Na^+-free glutamate uptake buffer at 37°C (Na^+, $n=5$), or standard glutamate uptake buffer with added 5 M L-*trans*-pyrrolidine-2,4-dicarboxylic acid at 37°C (PDC) ($n=5$). The tubes were then pre-incubated for 30 min at their respective temperatures. Following incubation, 10μM of unlabeled glutamic acid and 2 μCi of [H^3]-glutamate (Perkin Elmer Inc., Walther, MA) were then added to the samples for 10 min, with a final volume of each tube reaching 500 μL. The synaptosomal solution was then filtered through a cell harvester (Brandel, Gaithersburg, MD) with 0.9% cold saline solution and trapped on Whatman GF/C filters (GE Healthcare, Buckinghamshire, UK). The filters were then collected into scintillation vials, suspended in 5 mL of Ultima-Gold™ scintillation fluid (Perkin Elmer Inc., Waltham, MA) and counted on a scintillation counter (Beckman Coulter, LS 6500, Pasadena, CA).

Western blot analysis

Ten micrograms of total protein in 17 uL sample buffer (Invitrogen, Carlsbad, CA) were loaded into a pre-cast sodium dodecyl sulfate (SDS) gel with a 4–15% gradient (Mini-PROTEAN® TGX™ Bio-rad, Hercules, CA) and run at 180 V for 1 h, then transferred to polyvinylidene fluoride membranes (Bio-rad) at 16 V for 30 min. Membranes were blocked overnight in blocking buffer (Li-Cor, Lincoln, NE) and then incubated in primary antibodies (Abs; guinea-pig anti-GLT-1, AB1783 Millipore, Billerica, MA, dilution 1:5000; mouse anti-valosin-containing protein, AB11433 Abcam, Cambridge, MA, dilution 1:2500; rabbit anti-synaptophysin, AB23745 Abcam, dilution 1:50000) overnight at 4°C and then washed three times with tris-buffered saline (TBS). Near-infrared secondary antibodies were used at 1:5000, and blots were imaged on a Li-Cor Odyssey Imager as previously described.[26] We tested our Western blot assays using varying concentrations of total protein of rat brain tissue homogenate. These control studies demonstrated that our assays were linear for the protein concentrations used in our Western blot studies.

EM

Synaptosomal fragments were fixed in 1/2 Karnovsky fixative (2.5% paraformaldehyde and 2.0% glutaraldehyde in 0.1M Cacodylate buffer) and then post- fixed in 1% osmium tetroxide in 0.1M Caco buffer. Samples were then dehydrated in a graded series of ethanol, and infiltrated and embedded in Embed 812 resin. Following embedding, ultrathin sections were collected on copper mesh grids, post-stained with uranyl acetate and lead citrate, and examined using an FEI Tecnai T-12 electron microscope. All imaging was performed at the University of Alabama at Birmingham Electron Microscopy Core (Birmingham, AL).

Statistical analysis

All statistical tests were done with Prism version 6 (GraphPad Software Inc.). Data were tested for normality of distribution, and differences between conditions were assessed using one way analysis of variance (ANOVA) or *t* test, as appropriate. Post-hoc analysis was performed with Tukey's multiple comparison test when necessary. For all tests $\alpha=0.05$. All data are reported as mean value ± standard error of the mean (SEM).

Kinome array profiling

Profiling of serine-threonine kinome (STK) activity was performed using the PamStation12 microarray (PamGene International) and STK PamChips containing 144 consensus phosphopeptide sequences per well (4 of which are internal controls), immobilized on porous ceramic membranes. Each PamChip well was blocked with 2% bovine serum albumin (BSA) before 2 μg of protein in the manufacturer's kinase buffer (PamGene), 157 μM adenosine triphosphate (ATP), and FITC-labeled anti-phospho Ser/Thr antibodies (PamGene) were added in each well. The homogenized samples containing the active kinases and assay mix were pumped through the wells to facilitate interaction between kinases in the sample and specific peptide substrates immobilized on the chip. The degree of phosphorylation per well was measured in real time using Evolve (PamGene) kinetic image capture software. The software captures FITC-labeled anti-phospho antibodies binding to each phosphorylated peptide substrate every 6 sec for 90 min.[27] Primary analyses were performed from integrated exposure times for each spot (10 ms, 20 ms, 50 ms, 100 ms, and 200 ms) using steady state as quality control. Integrated spot intensities with the 99th percentile were used to calculate a minimal positive shift, and data were log2 transformed. These log-transformed spot intensities are the ''signal'' for each peptide. The signal intensities for each peptide were analyzed using BioNavigator 5.2 Software (PamGene).[27] Rodent brain samples evaluated here using the array are comparable to previous data acquired by us in human samples.[28]

A control array was run without the addition of ATP to identify nonspecific binding of labeled antibody to the array substrate (data not shown). Peptides with significant background signal in the -ATP condition (higher than the +ATP condition) were excluded from further analysis. Four peptide probes were excluded based on these criteria. Peptide probes for which signal was not detected in the +ATP condition were also excluded from analyses. Three additional peptides were excluded under this criterion, leaving a total of 133 peptide substrates.

Signal intensity data for each peptide (excluding the four control peptide substrates, three peptide substrates for whom kinase activity could not be detected, and four peptides with nonspecific activity) for all rodent samples was tested for outliers (± 2.5 SD from the mean), which were eliminated from our analyses. Comparisons for each peptide substrate were made using the mean values for each substrate for LFPI ($n=5$) and Sham ($n=5$) animals. The ratio of the means was used to calculate fold change for each peptide. Peptides with a fold change ±1.15 were considered significant for further analysis.

Identification of upstream kinases

Using Kinexus Phosphonet (Kinexus Bioinformatics) and GPS 2.1 prediction algorithms, we identified protein kinases acting on phosphorylation sites within the array peptide sequences.[29,30] These programs provide ranked predictions for serine-threonine kinases targeting putative phosphorylation sites in the peptide sequence. The top three kinases predicted by Kinexus and kinases with scores more than twice the prediction threshold for each phosphorylation site were included as predicted kinase ''hits'' for TBI-altered substrates. We then calculated the frequency of each kinase for the cortical and hippocampal data sets.

Random sampling analyses

To determine which upstream kinases are most likely to be important in the signaling network in acute TBI based on our kinome array data, we performed a random sampling analysis.[31,32] We generated data sets ($n=2000$) where each data point includes randomly selected reporter peptide substrates from the kinome array. Each data point in the analyses of frontal cortex included 25 substrates, matching the number of substrates with LFP-induced changes in kinase activity in the cortex. Each data point in the analysis of the HPC included 19 substrates, matching the number of substrates with LFP-induced changes in kinase activity in HPC.

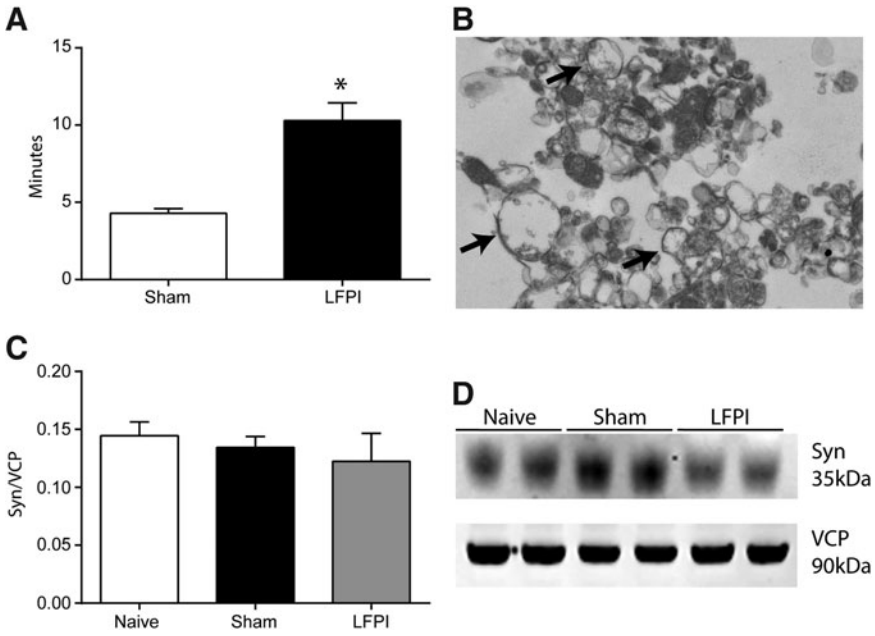

FIG. 1. Righting time following 2.0 atm lateral fluid percussion injury (LFPI) or sham surgery in adult male rats **(A)**. Electron micrograph of membrane vesicles isolated using density centrifugation from the prefrontal cortex **(B)** and expression of synaptophysin (Syn) protein in membrane vesicles from naïve, sham surgery, and LFPI rodents 24 h after injury (**C** and **D**). Data were normalized to valosin-containing protein (VCP) and expressed as mean ± SEM. $n = 5$ per group, $^*p < 0.05$.

Using Kinexus PhosphoNet and GPS 2.1 prediction algorithms, we identified kinases predicted to target each phosphorylation site on every array substrate, and then calculated the frequency of each kinase for all 2000 data points in cortical and hippocampal data sets. From these data we generated an ''expected'' distribution for each protein kinase. Means and standard deviations were calculated for each expected distribution. Kinases in the LFP data points with observed frequencies falling outside two standard deviations from the expected mean (derived from randomly generated data points) were carried forward into our network analyses.

Signaling network modeling

Kinases implicated by the random sampling analyses were used to create a model TBI signaling network. We generated a network model that 1) represents the number of direct interactions between protein kinase ''hits'' identified from our random sampling analyses, and 2) also represents other protein kinases in the Ingenuity Pathway database that have direct interactions with the these protein kinase ''hits.''[33] For the second group, we restricted the Ingenuity Pathway Analysis (IPA) grow tool to ''kinases'' and ''direct interactions'' and used the connect tool to create a kinase network.[33] The resulting output was refined by removing kinases with fewer than two connections to the emerging network. Because signaling networks may be amplified or muted based on the number of interactions between kinases, we weighted our model based on the number of interactions found for each kinase in the network.

IPA

The resulting TBI kinase network was further analyzed using IPA, as previously described, for associated upstream regulating factors and physiological functions.[28]

Exploratory kinome array studies.

For the inhibitor studies, 10 ug protein from each of the LFPI ($n = 5$) and Sham ($n = 5$) rodents were pooled to make a single

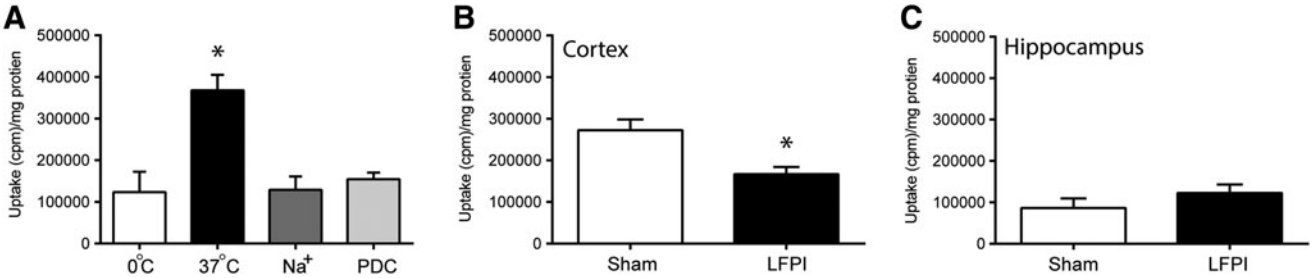

FIG. 2. ^{3}H-glutamate uptake in membrane vesicles isolated from adult rats 24 h after lateral fluid percussion injury (LFPI) or sham surgery. Low temperature (0°C), absence of sodium (Na^+), and the excitatory amino acid transporter inhibitor L-*trans*-pyrrolidine-2,4-dicarboxylate (PDC) all inhibited uptake compared with the 37°C positive control **(A)**. ^{3}H-glutamate uptake in membrane vesicles isolated from the prefrontal cortex **(B)** and hippocampus **(C)** 24 h following LFPI or sham. Data expressed as mean counts per minute ± SEM. $n = 5$ per group, $^*p < 0.05$.

pooled TBI sample and a single pooled Sham sample. Each sample was evaluated with the kinome array as previously described in the presence and absence of specific inhibitors for protein kinase B (Akt; Calbiochem 124005), c-Jun N-terminal kinase (JNK; SP600125, Calbiochem), and mitogen-activated protein kinase kinase (MEK; D-erythro-sphingosine N-hexanoyl, Calbiochem) plus protein kinase C (PKC; Bisindoylmaleimide Hydrochloride, Cell Signaling) at a final concentration of 150 uM.[28] PKC and MEK were combined because of limited space on the array plate (and we chose to prioritize Akt and JNK in this study for theoretical reasons). The ratio of kinase activity in the inhibitor/no inhibitor samples for each peptide substrate was used to calculate fold change data. Difference in fold change was calculated as follows: [(LFPI with inhibitor)/ (LFPI without inhibitor)] –[(Sham with inhibitor)/(Sham without inhibitor)]. Only protein substrates from the kinome array with detectable signal in Sham and LFPI samples were included in the inhibitor study analyses.

Results

Rats that received LFPI exhibited a significantly longer duration of latency for return of the righting reflex, a measurement of transient unconsciousness, than did their sham-operated counterparts ($t[8] = 5.096$, $p < 0.05$) (Fig. 1A). This indicates that TBI-induced loss of consciousness above and beyond that induced by anesthesia alone. Additionally, the duration of unconsciousness is similar to that observed with moderate TBI in this model.[22] We next confirmed the ultrastructural contents of our biochemical fractionation protocol. Membrane vesicles isolated using density centrifugation were imaged using EM (Fig. 1B). We found circular membranous structures with areas of pre- and post-synaptic density joining (black arrows). Expression levels of the synaptic marker synaptophysin did not significantly differ between experimental conditions ($F[2,11] = 0.439$, $p = 0.66$) (Fig. 1C and D).

We next evaluated glutamate uptake in membrane vesicles isolated from rats 24 h after LFPI. ^{3}H-glutamate uptake was temperature and sodium dependent, and was diminished by the excitatory amino acid transporter inhibitor L-*trans*-pyrrolidine-2, 4-dicarboxylate (PDC) ($F(3,16) = 10.90$, $p < 0.05$) (Fig. 2A). ^{3}H-glutamate uptake was lower (39%) in membrane vesicles isolated from the injured cortical hemisphere of LFPI rats than in sham surgery controls ($t[8] = 3.43$, $p < 0.05$) (Fig. 2B). We detected no differences in ^{3}H-glutamate uptake in membrane vesicles isolated from the HPC (Fig. 2C). To determine if changes in ^{3}H-glutamate uptake in the cortex were secondary to decreased GLT-1 expression versus other mechanisms, we measured GLT-1 protein levels using Western blot analysis. We did not detect any changes in total (monomer and dimer) GLT-1 protein levels in the prefrontal cortex or HPC in brain homogenate (Fig. 3A and B) or membrane vesicles (data not shown).

Since glutamate transport activity is potently regulated by protein kinases, we used a kinome array platform to explore global changes in kinase activity in LFPI. In the prefrontal cortex, 17 peptide substrates had increased phosphorylation levels ≥1.15-fold 24 h after LFPI compared controls, whereas eight peptides were ≥1.15-fold (Table 1). In the HPC, three peptide substrates were increased ≥1.15-fold, whereas 16 peptides were decreased ≥1.15-fold following TBI (Table 2).

Using publicly available databases, we mapped protein kinases specific for the peptide substrates from the kinome array, and performed permutation analyses to identify kinases across the reporter peptide data set with a high probability of being true positives (Table 3). We randomly generated a data set for each kinase

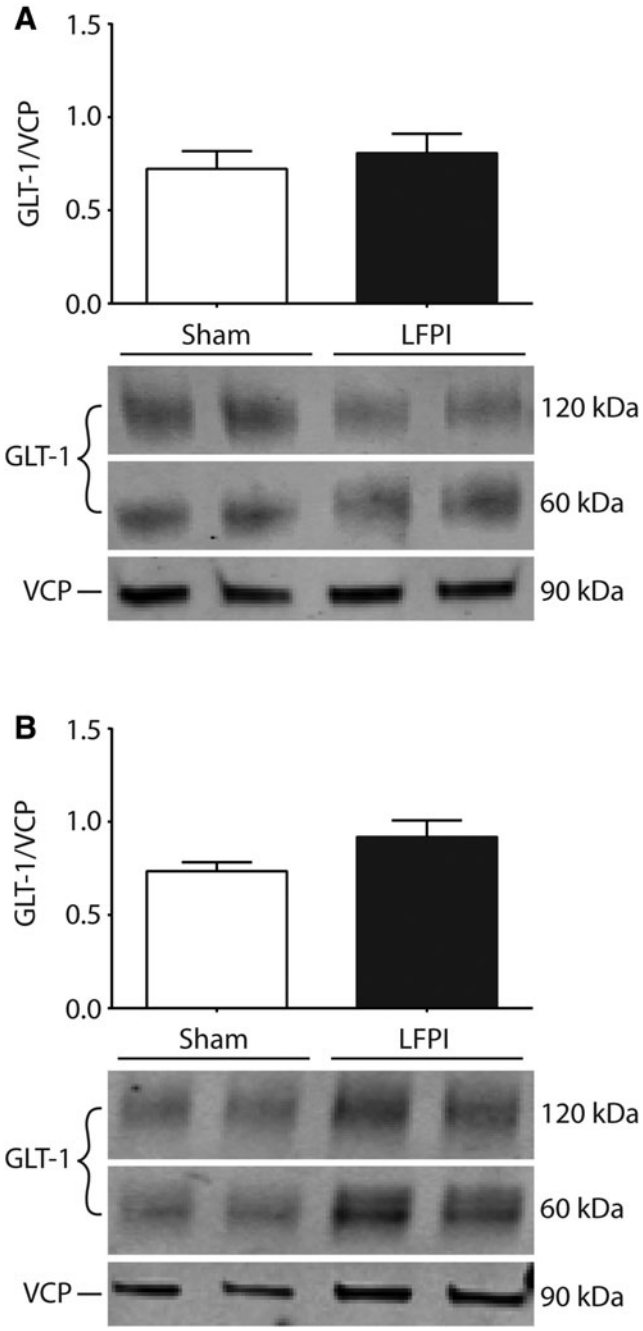

FIG. 3. Expression of excitatory amino acid transporter 2 (glutamate transporter-1 [GLT-1]) protein in brain homogenate from rats that had had lateral fluid percussion injury (LFPI) and sham surgery 24 h after injury in the prefrontal cortex **(A)** and hippocampus **(B)**. Data were normalized to valosin-containing protein (VCP) and expressed as mean ± SEM. $n = 5$ per group.

($n = 2000$) in which each data point reflected peptide substrates randomly selected from the kinome array. For the prefrontal cortex, we randomly selected 25 substrates for each data point, and for the HPC we randomly selected 19. We then made a frequency plot of the number of times a mapped kinase appeared in each randomly generated sample (Fig. 4, open bars). To be considered a true positive and carried forward into our network model, a kinase had to have an experimentally determined mapping frequency more

Table 1. Substrate Peptides Differentially Phosphorylated Between Lateral Fluid Percussion Injury and Sham in Frontal Cortex on the Kinome Array

Increased signal	*UniProt accession*	*Abbreviation*	*Fold change*	*Selected mapped kinases*
B-2 adrenergic receptor	P07550	ADRB2	1.16	MSK CAMK4 Akt CAMK2
Annexin1	P04083	ANXA1	1.22	PKG RSK Akt PKA
Cystic fibrosis transmembrane conductance regulator	P13569	CFTR	1.21	CDK GRK PKD PKA
Choriogonadotropin subunit beta	P01233	CGB	1.17	MSK PKG Akt GRK MEK
Colony-stimulating factor 1 receptor	P07333	CSF1R	1.25	PIM PKG DMPK PAK
Phospholemman ion transport regulator	O00168	FXYD1	1.22	PKA PKC CAMK2 MLK
G protein-coupled receptor 6	P46095	GPR6	1.26	GRK PKC PKG RSK
G protein signaling modulator	P81274	GPSM2	1.31	PKA RSK CAMK1 CAMK2
Glycogen (starch) synthase, liver	P54840	GYS2	1.20	PKA CASK RSK Akt
Potassium voltage-gated channel A1	Q09470	KCNA1	1.29	PKA ERK RSK CASK
Potassium voltage-gated channel A2	P16389	KCNA2	1.32	GRK RSK CAMK1 CASK
Potassium voltage-gated channel A3	P22001	KCNA3	1.32	GRK DMPK IKK MLK
Potassium voltage-gated channel B1	Q14721	KCNB1	1.17	DMPK GRK PKC PKG
Neutrophil cytosolic factor	P14598	NCF	1.17	PIM PKC MSK PAK
Phosphorylase kinase α1	P46020	PhKA1	1.16	PIM PKA SGK Akt
Protein tyrosine kinase 6	Q13882	PTK6	1.18	PAK GRK MAP2K PKD
v-raf viral oncogene	P04049	RAF1	1.23	AKT DMPK PKA PKC
v-rel viral oncogene	Q04864	REL	1.23	PIM PKG PKA DMPK
Decreased signal	*UniProt accession*	*Abbreviation*	*Fold change*	*Selected mapped kinases*
Branched chain ketoacid Dehydrogenase kinase	O14874	BCKDK	−1.19	SGK PRKX skMLCK RSK
ETS domain-containing protein Elk-1	P19419	ELK1	−1.34	GRK PKC PhK CDK
Kainate receptor 1	P39086	GRIK1	−1.84	GRK MLK ANP RSK
Lamin A	P02545	LMNA	−1.17	LKB MLK MK2/3 PIM
M-phase phosphoprotein 6	Q99547	MPHOSPH6	−1.15	JNK p38 ERK CDK
Neurotrophic tyrosine Kinase receptor 3	Q16288	NTRK3	−1.3	JNK CHEK1 CDK MLK
Retinoblastoma-like 2	Q08999	RBL2	−1.2	p38 JNK ERK CDK

MSK, mitogen- and stress-activated protein kinase; CAMK, calcium/calmodulin-dependent protein kinase; Akt, protein kinase B; PKG, protein kinase G; RSK, ribosomal s6 kinase; PKA, protein kinase A; CDK, cyclin-dependent kinase; GRK, G protein-coupled receptor kinase; PKD, protein kinase D; MEK, mitogen-activated protein kinase kinase; DMPK, dystrophia myotonica protein kinase; PAK, p21-activated kinase; PKC, protein kinase C; MLK, mixed lineage kinase; CASK, calcium/calmodulin-dependent serine protein *kinase*; ERK, extracellular signal-regulated kinase; IKK, I kappa B kinase; SGK, serum/glucocorticoid regulated kinase; MAP2K, mitogen-activated protein kinase kinase; PRKX, protein kinase X-linked; skMLCK, skeletal muscle myosin light chain kinase; PhK, phosphorylase *kinase;* ANP, atrial natriuretic peptide; LKB, liver kinase B; MK2/3, MAPK-activated protein kinases 2 and 3; JNK, c-Jun N-terminal kinase; p38, p38 mitogen-activated protein kinase; CHEK1, checkpoint kinase 1; ETS, E26 transformation-specific.

than two standard deviations from the mean of the randomly generated data set (Fig. 4, red lines). Nine protein kinases met this threshold in the prefrontal cortex, whereas four met this threshold in the HPC (Table 3).

We next used these high-yield kinases to construct signaling network interaction models for the prefrontal cortex and the HPC. We constructed a kinase interaction network model based on known interactions between kinases identified from our 24 h post-LFPI studies (Table 3) and the IPA database (gray circles and darker lines). We also modeled the up- and downstream kinases associated with our ''hits'' from Table 3 (white circles and lighter lines). The size of the circles reflects a smaller or larger number of interactions in the model. Kinases with the largest circles, including Akt and p21-activated kinases (PAK) in the cortex (Fig. 5) and PKC and protein kinase A (PKA) in the HPC (Fig. 6) are predicted to have the most involvement in the lesion and may be provisionally identified as signaling nodes in acute TBI.

We performed exploratory inhibitor studies in frontal cortex using the kinome array platform to investigate the regulation of several kinases implicated in TBI pathophysiology. To ensure that we were investigating drug effects, we increased our fold change threshold to ±1.5. Using this standard, kinase activity was decreased on 13 substrates in the Sham sample and 6 substrates in the LFPI sample, whereas activity increased on 6 substrates in the Sham sample and 16 substrates in the LFPI sample in the presence of the Akt inhibitor (Fig. 7A, left column). JNK inhibition decreased kinase activity on 20 substrates in the Sham sample and 4 substrates in the LFPI sample (Fig. 7A, center column). Kinase activity increased on no Sham substrates and on nine LFPI substrates in the presence of JNK inhibitor. Kinase activity was decreased on 41 and 46 substrates in the Sham and LFPI samples, respectively, by the combination of PKC and MEK inhibitors (Fig. 7A, right column). Kinase activity increased on 20 substrates in the Sham sample and on 10 substrates in the LFPI sample in the presence of the PKC-MEK inhibitor combination.

To investigate this further, we plotted the difference between the (+) inhibitor and the (-) inhibitor values LFPI and Sham for each reporter peptide (the change in fold change, Fig. 7B). Peptide substrates with a change in fold change of >0.5 were deemed to be differentially phosphorylated. Peptide substrates on the array that were not differentially phosphorylated are plotted as gray circles (-0.5 to 0.5). The Akt and JNK inhibitors yielded 41% and 29%

Table 2. Substrate Peptides Differentially Phosphorylated Between Lateral Fluid Percussion Injury and Sham in the Hippocampus on the Kinome Array

Increased signal	*UniProt accession*	*Abbreviation*	*Fold change*	*Selected mapped kinases*
B-2 adrenergic receptor	P07550	ADRB2	1.17	MSK CAMK4 Akt CAMK2
Branched chain ketoacid Dehydrogenase kinase	O14874	BCKDK	1.2	SGK PRKX skMLCK RSK
Serine/threonine-protein kinase Chk2	O96017	CHEK2	1.17	TBK1 IKK PIM PLK
Cyclic AMP-responsive element-binding protein 1	P16220	CREB1	1.16	PKA PKC RSK CAMK1
ETS domain-containing protein Elk-1	P19419	ELK1	1.15	PKA PKC RSK CAMK1
Kainate receptor 1	P39086	GRIK1	2.23	GRK MLK ANP RSK
Potassium voltage-gated channel subfamily A member 6	P17658	KCNA6	1.19	Akt DMPK PKA PDK
Phosphorylase kinase α1	P46020	PHKA1	1.19	PIM PKA SGK Akt
Cardiac phospholamban	P26678	PLN	1.17	RSK PKC GRK DMPK
Decreased signal	*Uniprot accession*	*Abbreviation*	*Fold change*	*Selected mapped kinases*
Potassium voltage-gated channel B1	Q14721	KCNB1	−1.22	DMPK GRK PKC PKG
Kinesin family 2C	Q99661	KIF2C	−1.17	PKC PAK GRK PKD
Protein kinase C beta type	P05771	PRKCC	−1.18	PKA PKC KIS RSK
v-raf viral oncogene	P04049	RAF1	−1.17	Akt DMPK PKA PKC
v-rel viral oncogene	Q04864	REL	−1.21	PIM PKG PKA DMPK
v-src sarcoma	P12931	SRC	−1.15	GRK MLK HCK BLK

MSK, mitogen- and stress-activated protein kinase; CAMK, calcium/calmodulin-dependent protein kinase; Akt, protein kinase B; PKG, protein kinase G; RSK, ribosomal s6 kinase; PKA, protein kinase A; GRK, G protein-coupled receptor kinase; PKD, protein kinase D; DMPK, dystrophia myotonica protein kinase; PAK, p21-activated kinase; PKC, protein kinase C; MLK, mixed lineage kinase; IKK, I kappa B kinase; SGK, serum/glucocorticoid regulated kinase; PRKX, protein kinase X-linked; skMLCK, skeletal muscle myosin light chain kinase; ANP, atrial natriuretic peptide; TBK, TANK-binding kinase; PLK, polo-like kinase; PDK, phosphoinositide-dependent kinase; KIS, *kinase* Interacting with stathmin; HCK, hematopoietic cell *kinase*; BLK, B lymphocyte kinase; ETS, E26 transformation-specific.

differentially phosphorylated substrates, respectively. The vast majority of these, 93% and 88%, were substrates for which changes in activity were in the opposite directions (solid black circles) between LFPI and SHAM samples. With combined PKC-MEK inhibition, 49% of substrates were differentially phosphorylated, however the majority of these (61%) represent differences in magnitude of fold change in the same direction (open circles). Panels C and D are representative kinetic curves of selected kinases from the array with and without inhibitor (Fig. 7).

Finally, we performed IPA analyses on the kinases included in the models for the cortex (Fig. 5) and HPC (Fig. 6). Kinases identified in the cortex were primarily associated with cell death and apoptosis pathways, whereas in the HPC, kinases were associated with apoptosis, proliferation, cytoskeletal remodeling, and cell cycle progression (Table 4).

Discussion

The results from these experiments point to a deficit in the function of glutamate transporters following TBI that is independent of changes in protein concentration, and may be mediated by aberrant activity of signaling pathways. Western blot analysis demonstrated no differences in GLT-1 protein expression in either cortical or hippocampal homogenates (Fig. 3A and B) 24 h following experimentally induced (2.0 atm) LFPI. However, membrane vesicles isolated from rats 24 h after brain injury exhibited decreased ^{3}H-glutamate uptake in the cortex, indicating diminished capacity to effectively remove glutamate from the extracellular space (Fig. 2B). Because we did not find changes in total GLT-1 protein levels, these results suggest a mechanism other than proteolysis, and/or decreased *de novo* expression. As kinases and other signaling molecules are potent regulators of glutamate transporters, we investigated the role of kinase activity on transporter function. Results from the kinome array studies indicate that multiple kinase signaling pathways are altered 24 h after LFPI. Our data yielded a TBI-associated signaling network that included nodes for Akt, PKC, and mechanistic target of rapamycin (mTOR) kinases. Because many of these kinase pathways are known regulators of GLT-1 function in uninjured tissue, we postulate that changes in signaling networks account for the diminished uptake capacity we observed in the cortex in acute TBI.[34–37]

The results of our experiments point to a deficit in glutamate reuptake without a concomitant reduction in transporter expression in either the cortex (Fig. 3A) or HPC (Fig. 3B). Multiple studies demonstrate altered expression of glutamate transporters following TBI; however, these effects vary based on the animal model used to induce the injury.[38] CCI models of injury consistently demonstrate downregulation of cortical and hippocampal expression of GLT-1, as well as decreases in mRNA levels for the transporter beginning 4–6 h after injury, and persisting for up to 72 h.[9,19,39] However, studies using LFPI have found mixed effects on glutamate transporter expression levels. Whereas there are reports of decreased (29%) GLT-1 expression in the ipsilateral cortex at 7 days post-injury,[21] other studies detected no changes in cortical expression of the transporter up to 24 h post-injury, and found increases in hippocampal GLT-1 expression across the same time period.[40] The discrepancies between these models may be a result of differences in injury location, mode or severity of the injury, the focal nature of

Table 3. Predicted Kinases in Frontal Cortex and Hippocampus After Lateral Fluid Percussion Injury

Frontal cortex					
Kinase	*Observed hits*	*Distribution dean*	*Standard deviation (SD)*	*Z score*	*Confidence interval*
Confidence interval ≥2 SD					
CAMK4	7	2.56	1.36	3.26	–0.16–5.28
CAMK2	14	8.25	2.08	2.77	4.09–12.41
GRK	15	9.26	2.16	2.66	4.94–13.58
PAK	9	4.66	1.77	2.45	1.12–8.21
Akt	10	5.68	1.91	2.27	1.86–9.49
PKD	5	2.18	1.30	2.18	–0.41–4.77
CK	8	4.35	1.72	2.13	0.91–7.78
DMPK	11	6.79	2.01	2.10	2.77–10.80
NEK	3	1.10	0.93	2.05	–0.75–2.95
Confidence interval between 1.5 and 2.0 SD					
mTOR	4	7.76	2.05	1.83	3.66–11.85
DAPK	2	5.15	1.86	1.69	1.42–8.88
PKA	13	9.51	2.14	1.63	5.22–13.79
PKG	10	6.80	2.01	1.59	2.78–10.82
Hippocampus					
Kinase	*Observed hits*	*Distribution mean*	*Standard deviation*	*Z score*	*Confidence interval*
Confidence interval ≥2 SD					
DMPK	8	4.07	1.63	2.41	0.80–7.33
PKA	10	5.70	1.80	2.40	2.11–9.29
mTOR	1	4.70	1.73	2.14	1.25–8.16
PKC	10	6.34	1.79	2.04	2.76–9.92
Confidence interval between 1.5 and 2.0 SD					
GRK	9	5.56	1.76	1.96	2.03–9.08
CK	0	2.65	1.37	1.94	–0.09–5.39
CAMK2	8	4.95	1.72	1.78	1.51–8.38
PKD	3	1.26	1.02	1.70	–0.79–3.31
PRXX	3	1.35	1.05	1.57	–0.76–3.45
CDK	5	7.86	1.84	1.55	4.17–11.24

CAMK, calcium/calmodulin-dependent protein kinase; GRK, G-protein coupled receptor kinase; PAK, p21-activated kinase; Akt, protein kinase B; PKD, protein kinase D; CK, casein kinase; DMPK, dystrophia myotonica-protein kinase; NEK, never in mitosis gene A-related kinase; mTOR, mechanistic target of rapamycin; DAPK, death-associated protein kinase; PKA, protein kinase A; PKG, protein kinase G; PKC, protein kinase C; PRKX, protein kinase, X-linked; CDK, cyclin-dependent kinase.

the CCI model, the recruitment of different second messenger signals, or a combination of these factors.[3,8] Studies in astrocyte cultures found that the half-life of GLT-1 is >24 h[41]; therefore the observed decreases in protein expression in the hours immediately following CCI[39] cannot be accounted for solely by diminished *de novo* expression of the transporter.

A possible explanation for the reduction in transporter activity following TBI involves the activity of caspase-3.[42] Caspase-3 cleaves GLT-1 at aspartate 505, a highly conserved cytosolic C-terminal site present on mouse, rodent, and human isoforms of the transporter.[10] Caspase-3 levels are increased in mammalian models of TBI.[43] Cleavage of GLT-1 by caspase-3 is dependent on caspase-3 concentration and results in a significant loss of function of the transporter; however, based on the epitope for our GLT-1 antibody, the truncated form is detectible on immunoblots, and we did not detect a band at this predicted relative migration distance in our Western blot studies.[10] This finding prompted us to evaluate changes in glutamate uptake in membrane vesicles and to explore other mechanisms that may alter GLT-1 activity.

To our knowledge, only one other study has previously characterized changes in glutamate uptake in a membrane preparation following experimental TBI.[44] This study found decreased glutamate uptake into synaptosomal membranes in the frontal cortex and HPC in the CCI model that persisted for at least 24 h after injury.[44] These deficits were detected in comparison to the contralateral hemisphere of the injured animals.[44] Although these findings are consistent with the changes we found in the frontal cortex, this prior study did not examine GLT-1 protein levels, leaving the question of whether the decrease in uptake was secondary to a decrease in GLT-1 expression.

One possible explanation for the deficit in glutamate uptake capacity is alterations in signaling networks following TBI. The current study is limited somewhat by a lack of available reagents. Specific phospho-GLT-1 antibodies are not available, and we are not able to directly assess phosphorylation status of GLT-1. Nor are we able to directly assess kinase activity on GLT-1 as a target substrate, because GLT-1 is not present on the array. However, GLT-1 expression can be upregulated through activation of Akt and extracellular signal-regulated kinase (ERK) signaling pathways, likely downstream of receptor tyrosine kinase (RTK) activation.[45–49] GLT-1 expression and function is also modulated by PKC.[50–53] Activation of PKC signaling rapidly decreases cell-surface expression of GLT-1 without decreasing total cellular GLT-1 protein levels, whereas activation of PKA modulates transporter function.[52–55] Therefore, alterations in the balance of signaling

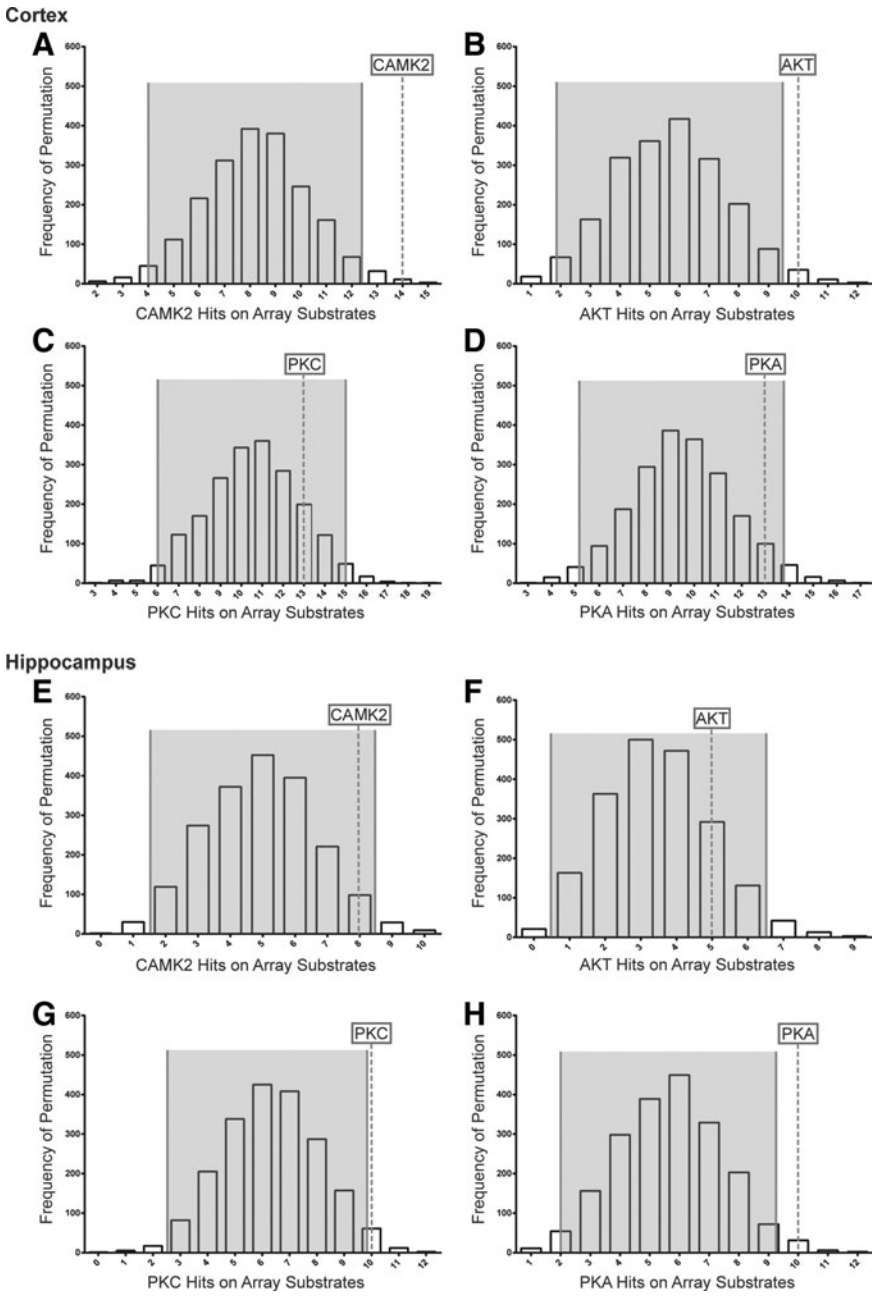

FIG. 4. Distribution plots of selected kinases for the cortex (**A–D**) and hippocampus (**E–H**) from permutation analyses of upstream kinases identified by kinome array 24 h following lateral fluid percussion injury (LFPI). Data represent the frequency of kinases mapped to substrates from the PamGene kinome array with ±1.15-fold difference in activity in the LFPI group compared with the Sham group. The open columns represent the random probability plot for the frequency of a selected upstream kinase ($n = 2000$). Dashed lines indicate the number of times the kinase actually appears in the cortex or hippocampus kinome data set. Gray area indicates ±2 SDs from the mean of the probability plot. CAMK2, calcium/calmodulin-dependent protein kinase type 2; Akt, protein kinase B; PKC, protein kinase C; PKA, protein kinase A.

molecules regulating transporter expression and/or function may represent a potent mechanism for glutamate transporter dysfunction after TBI. Supporting this hypothesis, we found changes in kinase activity for peptide substrates targeted by several serine/threonine kinases. Our bioinformatic analyses yielded a signaling network model that includes several kinases previously implicated in rodent models of TBI, including Ca^{2+}/calmodulin-dependent protein kinase (CAMK)4, CAMK2, PAK, Akt, protein kinase D (PKD), casein kinase (CK), PKA, mTOR, and PKC. The only kinase common to both regions examined (at the highest threshold) was dystrophia myotonica protein kinase (DMPK) (Table 3). Three kinases (G protein-coupled receptor kinase [GRK], DMPK, and never in mitosis gene A-related kinase [NEK]) from our network model were not previously implicated in TBI. Given that we did not find changes in glutamate uptake in the HPC, it is not surprising that kinase network modeling yielded different kinase nodes with a more extensive imputed network in the frontal cortex, where we found a decrease in glutamate uptake.

The kinase with the most interactions in our frontal cortex signaling model was Akt. Several studies have previously investigated

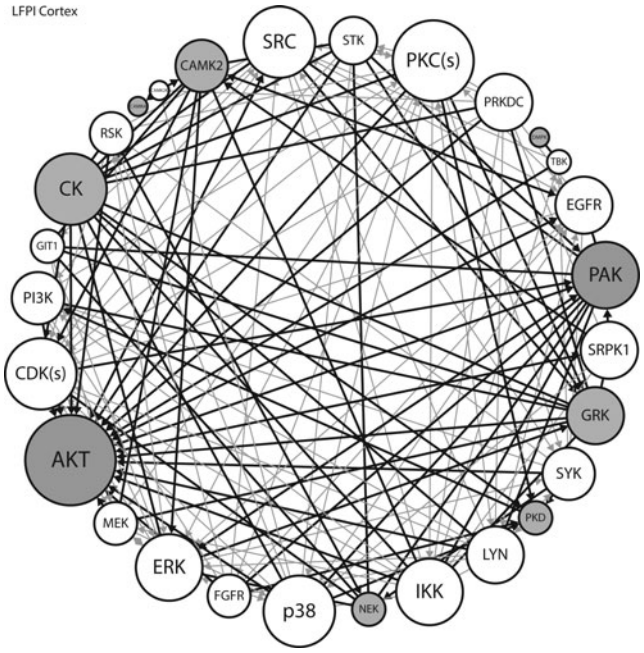

FIG. 5. For the frontal cortex kinome array data, kinases implicated by the random sampling analyses in Table 3 (gray circles) were combined with upstream kinases (white circles) to create a kinase network model. Using Ingenuity, kinases directly acting on our kinases of interest (thicker lines) were added to the network. Finally, Ingenuity was used to identify known interactions among all members of the network (thinner lines). Circle size corresponds to the number of interactions (larger circles have more interactions). PAK, p21-activated kinases; PKD, protein kinase D; GRK, G-protein coupled receptor kinase; DMPK, dystrophia myotonica-protein kinase; CK, casein kinase; NEK, never in mitosis gene A-related kinase; PKC, protein kinase C; Akt, protein kinase B; CDK, cyclin-dependent kinase; p38, p38 mitogen-activated protein kinase; CAMK2, calcium/calmodulin-dependent protein kinase type 2; CAMK4, calcium/calmodulin-dependent protein kinase type 4; MEK, mitogen-activated protein kinase kinase; ERK, extracellular signal-regulated kinase; GIT1, GPCR kinase-interacting protein 1; SRC, proto-oncogene tyrosine-protein kinase SRC; TBK, TANK-binding kinase; EGFR, epidermal growth factor receptor; IKK, I kappa B kinase; SYK, spleen tyrosine kinase; STK, serine/threonine kinase; PRKDC, DNA-dependent protein kinase; SRPK1, serine and arginine rich splicing factor (SRSF) protein kinase 1; LYN, tyrosine-protein kinase Lyn; FGFR, fibroblast growth factor receptors; PI3K, phosphoinositide 3-kinase; RSK, ribosomal s6 kinase; CAMK2K, calcium/calmodulin-dependent protein kinase kinase 2.

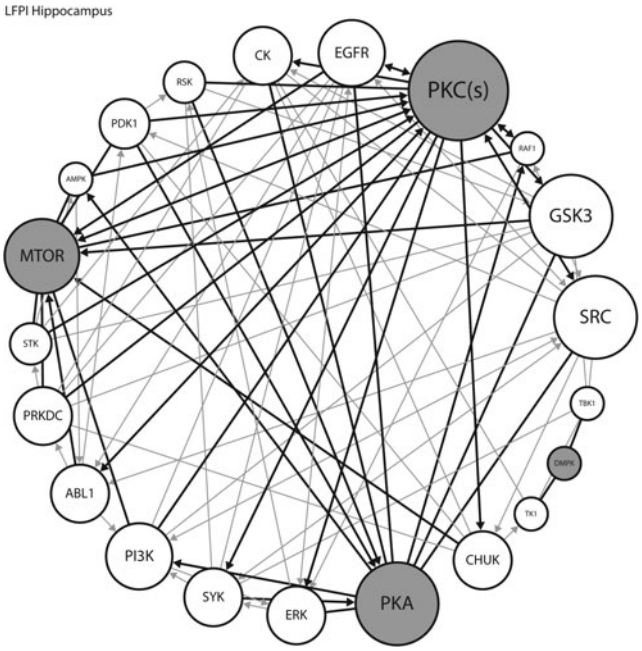

FIG. 6. For the hippocampus kinome array data, kinases implicated by the random sampling analyses in Table 3 (gray circles) were combined with upstream kinases (white circles) to create a kinase network model. Using Ingenuity, kinases directly acting on our kinases of interest (thicker lines) were added to the network. Finally, Ingenuity was used to identify known interactions among all members of the network (thinner lines). Circle size corresponds to the number of interactions (larger circles have more interactions). DMPK, dystrophia myotonica-protein kinase; PKA, protein kinase A; PKC, protein kinase C; PI3K, phosphoinositide 3-kinase; PDK1, phosphoinositide-dependent kinase 1; SRC, proto-oncogene tyrosine-protein kinase SRC; RAF1, rapidly accelerated fibrosarcoma; SYK, spleen tyrosine kinase; TBK1, TANK-binding kinase 1; GSK3, glycogen synthase kinase 3; ERK, extracellular signal-regulated kinase; PRKDC; DNA-dependent protein kinase; STK, serine/threonine kinase; RSK, ribosomal s6 kinase; CK, casein kinase; EGFR, epidermal growth factor receptor; TK1, thymidine kinase 1; CHUK, conserved helix-loop-helix ubiquitous kinase; ABL1, tyrosine-protein kinase ABL1; mTOR, mechanistic target of rapamycin; AMPK, 5' adenosine monophosphate-activated protein kinase.

the role of Akt in TBI. Changes in phospho-AKT (pAKT) protein levels were decreased, increased, or unchanged in areas outside of the injury site (HPC and cortex) 1–72 h post-injury.[34,36,37,56–60] Similarly divergent results were found at or near the injury site;[34,36,37,56–60] these disparate findings are likely the result of differences in TBI models, in assays for pAKT, and in cellular and subcellular expression patterns of AKT. For example, one study found decreased pAKT levels in the cytoplasm, but increases in the nucleus, with colocalization of pAKT and NeuN, suggesting these changes are primarily associated with neurons.[59] In addition, AKT is expressed and is active in astroglia, and differences in cell-specific expression could account for the variability in these reports, as there may be opposite changes in astrocytes versus neurons that reflect proximity to the injury as well as cell-specific pathophysiology. On balance, it appears that decreased pAKT expression may be a plausible mechanism for diminished GLT-1 activity in regions not directly injured. Interestingly, treatment with progesterone increased pAKT, providing a putative mechanism for restoring GLT-1 function.[61] Finally, there are several isoforms of Akt kinase, and the antibodies used for many of these studies do not differentiate between Akt1, Akt2, or Akt3.[62]

The kinase with the most interactions in our hippocampal signaling model was PKC; this kinase was also an indirect factor with a large number of interactions in our frontal cortex model. Several studies have investigated the role of PKC following TBI. No changes in PKC activity were detected 5–20 min after initiation of LFPI, but there was a shift in cytosolic to membrane-bound PKC α and β in the cortex, with a decrease only in the cytosolic fraction in the HPC.[63] A different study found increased PKC activity 1 h post-injury, with much higher increased PKC activity 3 h post-injury in the dorsal HPC, a region somewhat removed from the midline injury site.[35] An increase in membrane bound PKC was also

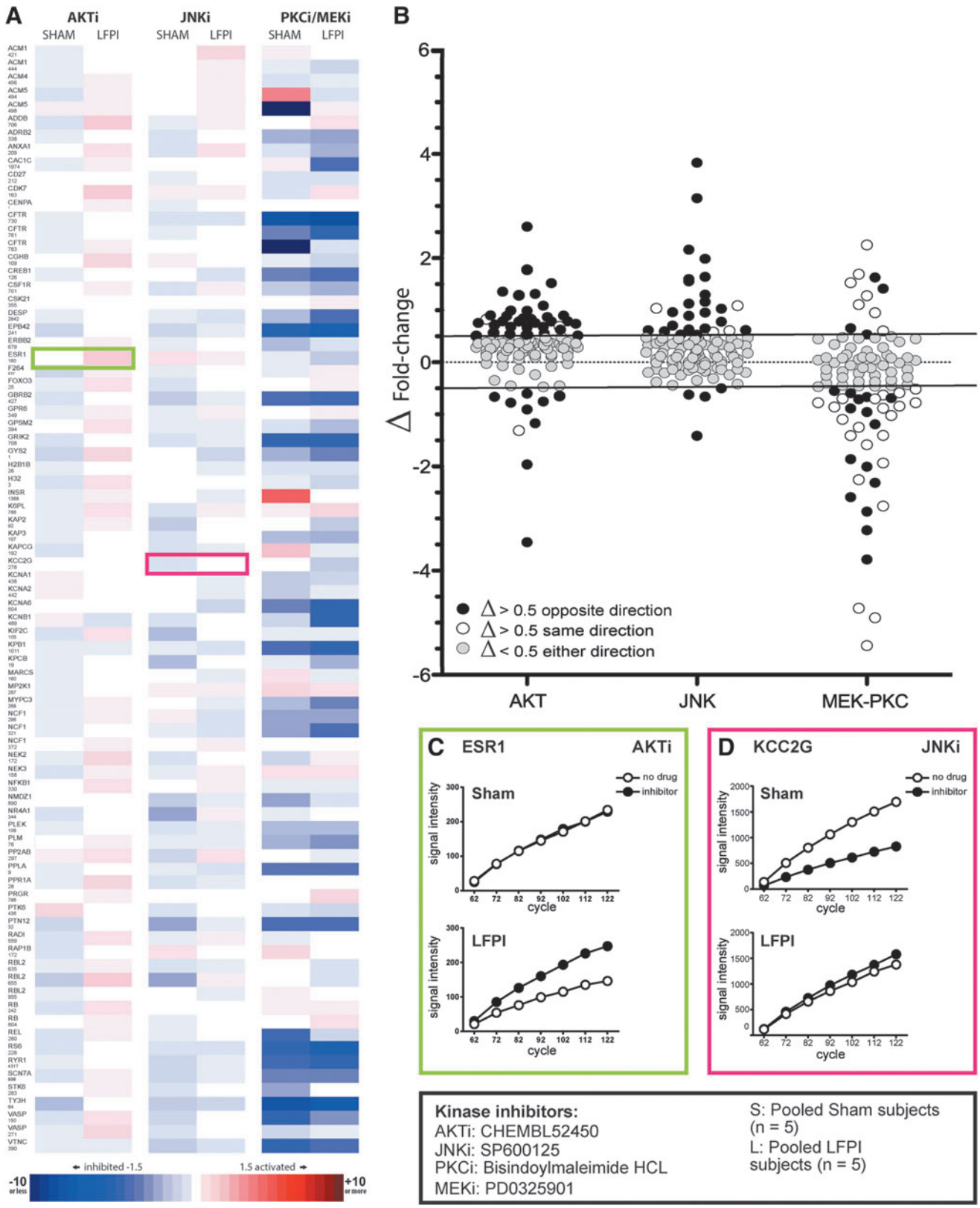

FIG. 7. Serine/threonine PamGene kinome array analysis of acute (24 h) pooled sham (Sham, $n = 5$) and lateral fluid percussion injury (LFPI, $n = 5$) cortical samples run in the presence and absence of specific inhibitors (i) for protein kinase B (Akt), c-Jun N-terminal kinase (JNK), mitogen-activated protein kinase kinase (MEK), and protein kinase C (PKC). **(A)** Heat map data is the ratio of the signal intensity of the sample with inhibitor:sample without inhibitor for pooled Sham or pooled LFPI samples. Lighter to darker blue indicates decreased phosphorylation (inhibition) of a specific array peptide, whereas lighter to darker red indicates increased phosphorylation (activation). **(B)** Scatter plots of the change in fold change {[(LFPI w/inhibitor)/ (LFPI w/o inhibitor)] – [(Sham w/inhibitor)/(Sham w/o inhibitor)]} for substrates from the kinome array with detectable signal in sham and LFPI samples. Substrates with a change in fold change >0.5 in the opposite direction are represented with black circles; those with >0.5 fold change in the same direction are represented with white circles. Gray circles indicate substrates with change in fold change <0.5 (regardless of valence). **(C)** and **(D)**, representative activity curves for select reporter peptides highlight the differential effects of inhibitors on kinase activity in Sham versus acute LFPI. **(C)** Estrogen receptor 1 (ESR1) signal ± AKTi, **(D)** Calcium/calmodulin-dependent protein kinase 2 (KCC2G) signal ± JNKi.

Table 4. Pathway Analyses: Predicted Regulating Factors with Kinases and Associated Functions

Name	*Abbrev.*	p *value*	*Kinases*	*Function*
Frontal cortex				
Huntington protein	HTT	7.20E-11	GRK; Akt; CK; CDK; CAMKII; CAMKIV	Cell death; apoptosis; degeneration
Activating transcription factor 3	ATF3	1.62E-7	CDK; NEK	Apoptosis; cell cycle progression
Retinoblastoma-like 1	RBL1	3.49E-7	CDK; NEK	Cell cycle progression; cytostasis; proliferation
Short stature homeobox	SHOX	6.80E-7	CDK	Cell cycle progression; apoptosis
Forkhead box M1	FOXM1	1.08E-6	CDK; NEK	Proliferation; cell cycle progression
Tumor protein 53	TP53	1.10E-6	GRK; Akt; CAMKII; CDK; PKD; PAK; NEK; CK	Apoptosis; cell cycle progression
Thyroid hormone receptor B	THRB	1.13E-6	Akt; CDK	Proliferation; abnormal morphology
Ubiquitin ligase E3A	UBE3A	9.09E-6	CAMKII; CDK	Capacitation; senescence;
Jun proto-oncogene	JUN	1.47E-5	Akt; CDK; PAK	Apoptosis; transformation; cell death
Hippocampus				
Glucocorticoid receptor	NR3C1	1.47E-6	PKA; PKC	Apoptosis; remodeling
Tumor protein 53	TP53	1.43E-5	PKA; PKC	Apoptosis; cell cycle progression
Sp1 transcription factor	SP1	9.63E-5	PKA; PKC; DMPK	Transcription; proliferation; cell death
Atrophin 1	ATN1	2.80E-4	PKA; PKC	Apoptosis; cell death; differentiation
Huntington protein	HTT	4.46E-4	mTOR; PKA; PKC	Cell death; apoptosis; degeneration
Myogenic differentiation 1	MYOD1	6.30E-4	PKA	Differentiation; cell cycle progression
ELAV-like family member 1	CELF1	9.63E-4	DMPK	Degeneration
Muscleblind-like splicing regulator	MBNL1	9.63E-5	DMPK	Alternative splicing; abnormal morphology; differentiation
Forkhead box D2	FOXD2	9.63E-6	PKA	Proliferation; axon extension
Runt-related transcrition factor	RUNX1	3.90E-3	PKC	Differentiation; proliferation; apoptosis

GRK, G-protein coupled receptor kinase; Akt, protein kinase B; CK, casein kinase; CDK, cycli-dependent kinase; CAMK, calcium/calmodulin-dependent protein kinase; NEK, never in mitosis gene A-related kinase; PKD, protein kinase D; PAK, p-21 activated kinase; PKA, protein kinase A; PKC, protein kinase C; DMPK, dystrophia myotonica-protein kinase; mTOR, mechanistic target of rapamycin.

detected at 3 h, but no changes in activity were found 24 h after LFPI in the HPC.[35] A third study found increased expression of PKC isoforms in the left prefrontal cortex 24 h following blast exposure TBI, with an increase in PKCε and a decrease in PKCα protein levels after treatment with the PKC modulator bryostatin-1.[64–66] These data were interpreted as indicating increased blood–brain barrier permeability.[64]

Similar to Akt, the cellular specificity, subcellular localization, and temporal changes in PKC localization and function will theoretically have a profound effect on GLT-1 function. The balance between GLT-1 promoting and GLT-1 diminishing pathways following TBI is highlighted by astrocyte cell cultures examining the effects of PKC. Long-term activation of PKC by phorbol esters in cultured cortical astrocytes results in overall decreases in GLT-1 expression, similar to that exhibited in a number of animal models of TBI.[19,67] In contrast to long-term activation of PKC, shorter term activity of the kinase results in sequestration of the transporter to an intracellular storage site by a clathrin-mediated endocytotic mechanism.[67] This intracellular sequestration of GLT-1 diminishes cell-surface expression, and thus would impact removal of glutamate from the extracellular space, but does not lead to an overall reduction in transporter expression. Our data are consistent with a signaling milieu that diminishes GLT-1 activity in the frontal cortex, but not HPC, 24 h after LFPI.

Several other kinases implicated in our signaling network were previously implicated in TBI models. For example, PKA activity was elevated in the medial prefrontal cortex (mPFC) following controlled cortical impact 7 and 14 days post-injury, with no change in expression levels of the catalytic (C-α) or regulatory (RI-α/ß) subunits.[68] In the HPC 1 h following lateral FPI, phospho-CAMKIV Thr196 and phospho-CAMKI Thr177 were increased, whereas pCAMKII was increased in membrane subcellular fractions from the parietal cortex fractions at 30 min, 4 h, and 24 h after injury.[69] Changes in CAMKII activity after TBI are particularly interesting, as the two isoforms of GLT-1, GLT-1a, and GLT-1b are differentially regulated *in vitro* by CAMKII.[70] Increases in CAMKII activity suggested by increased pCAMKII would destabilize GLT-1b membrane localization and accelerate EAAT2b turnover, altering glutamate uptake dynamics and neuronal activity.[70] These findings are consistent with our signaling network models, and suggest that regions outside of the direct injury site may be differentially affected by LFPI.

We performed exploratory kinase inhibitor studies using pooled samples from our 24 h LFPI experiments. In the frontal cortex, inhibition of Akt or JNK had markedly divergent effects on phosphorylation of peptide substrates on the kinome array in LFPI versus Sham animals. The kinome array readout is one that reflects the net effects of kinase activity in a complex biological sample. Inhibiting Akt and JNK activity in these complex samples led to broad-based decreases in phosphorylation in the Sham animals, as expected; surprisingly, a large number of peptide substrates had increased phosphorylation in the LFPI samples. Two mechanisms may explain these results. First, these kinases may be rendered insensitive to inhibition in the aftermath of injury. Second, and perhaps more likely, inhibition of these kinases facilitates nonselective phosphorylation by other active kinases in a severely dysregulated signaling landscape. Serine-threonine kinases target phosphorylation sites, in part, through the chemical properties of flanking amino acid sequences, but will readily target suboptimal sites when competition for those sites or additional specificity factors are lacking.[71] Overall, these results indicate that the signaling milieu in the frontal cortex is profoundly altered, and that regulatory mechanisms may be compromised acutely after TBI.

Treatment with a combination of PKC and MEK inhibitors primarily suppressed kinase activity, and the majority of differentially phosphorylated substrates were changes in magnitude in the same direction for the Sham versus LFPI groups. These findings suggest PKC-ERK signaling may be relatively intact and is consistent with our cortical signaling model, which directly implicates Akt, but not ERK, PKC, or MEK, as a major signaling node in TBI. Interestingly, pretreatment with a combination of Akt and mTOR inhibitors improved post-injury wire grip performance and hidden platform latencies, effects that may be mediated by elevated glycogen synthase kinase 3 beta (GSK3β) expression or activity in the HPC.[36]

There are several limitations to our study. All of our data were generated from tissue samples from whole brain regions that were blended. Because our samples included mixtures of all cell types found in the brain, we cannot assess the relative contributions of astroglia versus neurons, for example, when interpreting our data. This is particularly relevant for studies of GLT-1, as most cortical GLT-1 expression and activity is in astrocytes, whereas Akt is found in both neurons and astroglia. Cell-level kinome studies are needed to determine if the TBI signaling networks described in this study are cell specific. Our model administers an FPI to the ipsilateral parietal cortex; we examined the frontal cortex and HPC in our studies. Therefore, our results may differ from other reports that directly examined the injury site, and/or had more or less focal models, such as CCI or blast injury, respectively. Additional studies are required to determine whether GLT-1 expression is upregulated in neurons after injury, which could provide an explanation for some of our current findings. GLT-1 is primarily astrocytic with low GLT-1a expression in a subset of neurons. Studies in other models of CNS injury demonstrate phenotypic switching of typically ''astrocytic'' EAATs onto neuronal processes.[72] Upregulated EAAT expression in neurons could be a compensatory attempt by the brain to offset increases in extracellular glutamate following TBI; however, these efforts may ultimately harm neuronal tissue by making it more vulnerable to excitotoxicity because of intracellular glutamate levels beyond the buffering or metabolic capacity of neurons.[73] It remains to be determined whether GLT-1 function is regulated by direct interaction with implicated kinases. Additional studies using kinase inhibitors in synaptosomal preparations may help answer that question. Finally, our GLT-1 antibody detects both GLT-1a and GLT-1b isoforms. Future studies are required to determine the contributions of the two isoforms to the observed deficits in cortical glutamate uptake.

We found differential changes in glutamate uptake and signaling networks at sites removed from the direct injury site following LFPI. This regional specificity suggests that the HPC and frontal cortex may have different degrees and mechanisms of pathological responses, resilience, and/or sensitivity to injury. Building on this work, future studies should examine cell-level changes in signaling networks, with particular emphasis on astroglia versus neurons, particularly in regions where most glutamate uptake is facilitated by astroglia, such as the frontal cortex. Our data suggest that signaling networks in the HPC supporting GLT-1 activity are not perturbed, whereas the cortical signaling milieu is associated with diminished glutamate uptake; drawing on the field of cancer biology to explore the pharmacological effects of signaling network modulators may provide new substrates to reverse the changes in the frontal cortex and/or simulate the changes found in the HPC that may be protective.

Acknowledgments

This work was partially supported by R01NS075162 (C.L.F.).

Author Disclosure Statement

No competing financial interests exist.

References

1. Langlois, J.A., Rutland-Brown, W., and Wald, M.M. (2006). The epidemiology and impact of traumatic brain injury: a brief overview. J. Head Trauma Rehabil. 21, 375–378.
2. Bruns, J., Jr., and Hauser, W.A. (2003). The epidemiology of traumatic brain injury: a review. Epilepsia 44, Suppl. 10, 2–10.
3. Xiong, Y., Mahmood, A., and Chopp, M. (2013). Animal models of traumatic brain injury. Nat. Rev. Neurosci. 14, 128–142.
4. Katayama, Y., Becker, D.P., Tamura, T., and Hovda, D.A. (1990). Massive increases in extracellular potassium and the indiscriminate release of glutamate following concussive brain injury. J. Neurosurg. 73, 889–900.
5. Olney, J.W. (1990). Excitotoxicity: an overview. Can. Dis. Wkly Rep.16, Suppl. 1E, 47–57.
6. Nilsson, P., Hillered, L., Ponten, U., and Ungerstedt, U. (1990). Changes in cortical extracellular levels of energy-related metabolites and amino acids following concussive brain injury in rats. J. Cereb. Blood Flow Metab. 10, 631–637.
7. Faden, A.I., Demediuk, P., Panter, S.S., and Vink, R. (1989). The role of excitatory amino acids and NMDA receptors in traumatic brain injury. Science 244, 798–800.
8. Yi, J.H., and Hazell, A.S. (2006). Excitotoxic mechanisms and the role of astrocytic glutamate transporters in traumatic brain injury. Neurochem. Int. 48, 394–403.
9. van Landeghem, F.K., Stover, J.F., Bechmann, I., Bruck, W., Unterberg, A., Buhrer, C., and von Deimling, A. (2001). Early expression of glutamate transporter proteins in ramified microglia after controlled cortical impact injury in the rat. Glia 35, 167–179.
10. Boston–Howes, W., Gibb, S.L., Williams, E.O., Pasinelli, P., Brown, R.H., Jr., and Trotti, D. (2006). Caspase-3 cleaves and inactivates the glutamate transporter EAAT2. J. Biol. Chem. 281, 14,076–14,084.
11. Allen, N.J., Karadottir, R., and Attwell, D. (2004). Reversal or reduction of glutamate and GABA transport in CNS pathology and therapy. Pflugers Arch 449, 132–142.
12. Kanai, Y., and Hediger, M.A. (2003). The glutamate and neutral amino acid transporter family: physiological and pharmacological implications. Eur. J. Pharmacol. 479, 237–247.
13. Shigeri, Y., Seal, R.P., and Shimamoto, K. (2004). Molecular pharmacology of glutamate transporters, EAATs and VGLUTs. Brain Res. Rev. 45, 250–265.
14. Danbolt, N.C., Storm–Mathisen, J., and Kanner, B.I. (1992). An [Na+ + K+]coupled L-glutamate transporter purified from rat brain is located in glial cell processes. Neuroscience 51, 295–310.
15. Murphy–Royal, C., Dupuis, J.P., Varela, J.A., Panatier, A., Pinson, B., Baufreton, J., Groc, L., and Oliet, S.H. (2015). Surface diffusion of astrocytic glutamate transporters shapes synaptic transmission. Nat. Neurosci. 18, 219–226.
16. Tzingounis, A.V., and Wadiche, J.I. (2007). Glutamate transporters: confining runaway excitation by shaping synaptic transmission. Nat. Rev. Neurosci. 8, 935–947.
17. Velasco, I., Tapia, R., and Massieu, L. (1996). Inhibition of glutamate uptake induces progressive accumulation of extracellular glutamate and neuronal damage in rat cortical cultures. J. Neurosci. Res. 44, 551–561.
18. Rothstein, J.D., Dykes–Hoberg, M., Pardo, C.A., Bristol, L.A., Jin, L., Kuncl, R.W., Kanai, Y., Hediger, M.A., Wang, Y., Schielke, J.P., and Welty, D.F. (1996). Knockout of glutamate transporters reveals a major role for astroglial transport in excitotoxicity and clearance of glutamate. Neuron 16, 675–686.
19. Rao, V.L., Dogan, A., Bowen, K.K., Todd, K.G., and Dempsey, R.J. (2001). Antisense knockdown of the glial glutamate transporter GLT-1 exacerbates hippocampal neuronal damage following traumatic injury to rat brain. Eur. J. Neurosci. 13, 119–128.
20. Palmer, A.M., Marion, D.W., Botscheller, M.L., Swedlow, P.E., Styren, S.D., and DeKosky, S.T. (1993). Traumatic brain injury-induced excitotoxicity assessed in a controlled cortical impact model. J. Neurochem. 61, 2015–2024.
21. Goodrich, G.S., Kabakov, A.Y., Hameed, M.Q., Dhamne, S.C., Rosenberg, P.A., and Rotenberg, A. (2013). Ceftriaxone treatment after traumatic brain injury restores expression of the glutamate transporter,

GLT-1, reduces regional gliosis, and reduces post-traumatic seizures in the rat. J. Neurotrauma 30, 1434–1441.
22. Day, N.L., Floyd, C.L., D'Alessandro, T.L., Hubbard, W.J., and Chaudry, I.H. (2013). 17beta-estradiol confers protection after traumatic brain injury in the rat and involves activation of g protein-coupled estrogen receptor 1. J. Neurotrauma 30, 1531–1541.
23. McIntosh, T.K., Vink, R., Noble, L., Yamakami, I., Fernyak, S., Soares, H., and Faden, A.L. (1989). Traumatic brain injury in the rat: characterization of a lateral fluid-percussion model. Neuroscience 28, 233–244.
24. Sullivan, C.R., Funk, A.J., Shan, D., Haroutunian, V., and McCullumsmith, R.E. (2015). Decreased chloride channel expression in the dorsolateral prefrontal cortex in schizophrenia. PloS One 10, e0123158.
25. Whittaker, V.P. (1988). Synaptosome preparations. J. Neurochem. 50, 324–325.
26. Shan, D., Lucas, E.K., Drummond, J.B., Haroutunian, V., Meador–Woodruff, J.H., and McCullumsmith, R.E. (2013). Abnormal expression of glutamate transporters in temporal lobe areas in elderly patients with schizophrenia. Schizophr. Res. 144, 1–8.
27. Jarboe, J.S., Jaboin, J.J., Anderson, J.C., Nowsheen, S., Stanley, J.A., Naji, F., Ruijtenbeek, R., Tu, T., Hallahan, D.E., Yang, E.S., Bonner, J.A., and Willey, C.D. (2012). Kinomic profiling approach identifies Trk as a novel radiation modulator. Radiother. Oncol. 103, 380–387.
28. McGuire, J.L., Hammond, J.H., Yates, S.D., Chen, D., Haroutunian, V., Meador–Woodruff, J.H., and McCullumsmith, R.E. (2014). Altered serine/threonine kinase activity in schizophrenia. Brain Res. 1568, 42–54.
29. Xue, Y., Lieu, Z., Cao, J., Ma, Q., Gao, X., Wang, Q., Jin, C., Zhou, Y., Wen, L., and Ren, J. (2011). GPS 2.1: enhanced prediction of kinase specific phosphorylation sites with an algorithm of motif length selection. Protein Eng. Des. Sel. 24, 6.
30. Safaei, J., Manuch, J., Gupta, A., Stacho, L., and Pelech, S. (2011). Prediction of 492 human protein kinase substrate specificities. Proteome Sci. 9, Suppl. 1, S6.
31. Ludbrook, J. (1994). Advantages of permutation (randomization) tests in clinical and experimental pharmacology and physiology. Clin. Exp. Pharmacol. Physiol. 21, 673–686.
32. Ludbrook, J. (1995). Issues in biomedical statistics: comparing means by computer-intensive tests. Aust. N. Z. J. Surg. 65, 812–819.
33. Muurling, T., and Stankovic, K.M. (2014). Metabolomic and network analysis of pharmacotherapies for sensorineural hearing loss. Otol. Neurotol. 35, 1–6.
34. Noshita, N., Lewen, A., Sugawara, T., and Chan, P.H. (2002). Akt phosphorylation and neuronal survival after traumatic brain injury in mice. Neurobiol. Dis. 9, 294–304.
35. Yang, K., Taft, W.C., Dixon, C.E., Todaro, C.A., Yu, R.K., and Hayes, R.L. (1993). Alterations of protein kinase C in rat hippocampus following traumatic brain injury. J. Neurotrauma 10, 287–295.
36. Park, J., Zhang, J., Qiu, J., Zhu, X., Degterev, A., Lo, E.H., and Whalen, M.J. (2012). Combination therapy targeting Akt and mammalian target of rapamycin improves functional outcome after controlled cortical impact in mice. J. Cereb. Blood Flow Metab. 32, 330–340.
37. Farook, J.M., Shields, J., Tawfik, A., Markand, S., Sen, T., Smith, S.B., Brann, D., Dhandapani, K.M., and Sen, N. (2013). GADD34 induces cell death through inactivation of Akt following traumatic brain injury. Cell Death Dis. 4, e754.
38. Lauriat, T.L., and McInnes, L.A. (2007). EAAT2 regulation and splicing: relevance to psychiatric and neurological disorders. Mol. Psychiatry 12, 1065–1078.
39. Rao, V.L., Baskaya, M.K., Dogan, A., Rothstein, J.D., and Dempsey, R.J. (1998). Traumatic brain injury down-regulates glial glutamate transporter (GLT-1 and GLAST) proteins in rat brain. J. Neurochem. 70, 2020–2027.
40. Yi, J.H., Pow, D.V., and Hazell, A.S. (2005). Early loss of the glutamate transporter splice-variant GLT-1v in rat cerebral cortex following lateral fluid-percussion injury. Glia 49, 121–133.
41. Zelenaia, O.A., and Robinson, M.B. (2000). Degradation of glial glutamate transporter mRNAs is selectively blocked by inhibition of cellular transcription. J. Neurochem. 75, 2252–2258.
42. Gibb, S.L., Boston–Howes, W., Lavina, Z.S., Gustincich, S., Brown, R.H., Jr., Pasinelli, P., and Trotti, D. (2007). A caspase-3-cleaved fragment of the glial glutamate transporter EAAT2 is sumoylated and targeted to promyelocytic leukemia nuclear bodies in mutant SOD1-linked amyotrophic lateral sclerosis. J. Biol. Chem. 282, 32,480–32,490.
43. Zhang, J., Tao, D.Q., Zhao, H., and Yin, Z.Y. (2012). Expression of Hsp70 and Caspase-3 in rabbits after severe traumatic brain injury. Chin. J. Traumatol. 15, 338–341.
44. Sullivan, P.G., Keller, J.N., Mattson, M.P., and Scheff, S.W. (1998). Traumatic brain injury alters synaptic homeostasis: implications for impaired mitochondrial and transport function. J. Neurotrauma 15, 789–798.
45. Abe, K., Hosoi, R., Momosaki, S., Kobayashi, K., Ibii, N., and Inoue, O. (2002). Increment of in vivo binding of [3H]SCH 23390, a dopamine D1 receptor ligand, induced by cyclic AMP-dependent protein kinase in rat brain. Brain Res. 952, 211–217.
46. Figiel, M., Maucher, T., Rozyczka, J., Bayatti, N., and Engele, J. (2003). Regulation of glial glutamate transporter expression by growth factors. Exp. Neurol. 183, 124–135.
47. Gegelashvili, G., Dehnes, Y., Danbolt, N.C., and Schousboe, A. (2000). The high-affinity glutamate transporters GLT1, GLAST, and EAAT4 are regulated via different signalling mechanisms. Neurochem. Int. 37, 163–170.
48. Li, L.B., Toan, S.V., Zelenaia, O., Watson, D.J., Wolfe, J.H., Rothstein, J.D., and Robinson, M.B. (2006). Regulation of astrocytic glutamate transporter expression by Akt: evidence for a selective transcriptional effect on the GLT-1/EAAT2 subtype. J. Neurochem. 97, 759–771.
49. Zelenaia, O., Schlag, B.D., Gochenauer, G.E., Ganel, R., Song, W., Beesley, J.S., Grinspan, J.B., Rothstein, J.D., and Robinson, M.B. (2000). Epidermal growth factor receptor agonists increase expression of glutamate transporter GLT-1 in astrocytes through pathways dependent on phosphatidylinositol 3-kinase and transcription factor NF-kappaB. Mol. Pharmacol. 57, 667–678.
50. Casado, M., Bendahan, A., Zafra, F., Danbolt, N.C., Aragon, C., Gimenez, C., and Kanner, B.I. (1993). Phosphorylation and modulation of brain glutamate transporters by protein kinase C. J. Biol. Chem. 268, 27,313–27,317.
51. Daniels, K.K., and Vickroy, T.W. (1999). Reversible activation of glutamate transport in rat brain glia by protein kinase C and an okadaic acid-sensitive phosphoprotein phosphatase. Neurochem. Res. 24, 1017–1025.
52. Gonzalez, M.I., and Robinson, M.B. (2004). Protein kinase C-dependent remodeling of glutamate transporter function. Mol. Interv. 4, 48–58.
53. Kalandadze, A., Wu, Y., and Robinson, M.B. (2002). Protein kinase C activation decreases cell surface expression of the GLT-1 subtype of glutamate transporter. Requirement of a carboxyl-terminal domain and partial dependence on serine 486. J. Biol. Chem. 277, 45,741–45,750.
54. Adolph, O., Koster, S., Rath, M., Georgieff, M., Weigt, H.U., Engele, J., Senftleben, U., and Fohr, K.J. (2007). Rapid increase of glial glutamate uptake via blockade of the protein kinase A pathway. Glia 55, 1699–1707.
55. Guillet, B.A., Velly, L.J., Canolle, B., Masmejean, F.M., Nieoullon, A.L., and Pisano, P. (2005). Differential regulation by protein kinases of activity and cell surface expression of glutamate transporters in neuron-enriched cultures. Neurochem. Int. 46, 337–346.
56. Zhang, C., Zhu, J., Zhang, J., Li, H., Zhao, Z., Liao, Y., Wang, X., Su, J., Sang, S., Yuan, X., and Liu, Q. (2014). Neuroprotective and anti-apoptotic effects of valproic acid on adult rat cerebral cortex through ERK and Akt signaling pathway at acute phase of traumatic brain injury. Brain Res. 1555, 1–9.
57. Zhang, L., Ding, K., Wang, H., Wu, Y., and Xu, J. (2015). Traumatic brain injury-induced neuronal apoptosis is reduced through modulation of PI3K and autophagy pathways in mouse by FTY720. Cell. Molec. Neurobiol. 36, 131–142.
58. Zhang, X., Chen, Y., Ikonomovic, M.D., Nathaniel, P.D., Kochanek, P.M., Marion, D.W., DeKosky, S.T., Jenkins, L.W. and Clark, R.S. (2006). Increased phosphorylation of protein kinase B and related substrates after traumatic brain injury in humans and rats. J. Cereb. Blood Flow Metab. 26, 915–926.
59. Zhao, S., Fu, J., Liu, F., Rastogi, R., Zhang, J., and Zhao, Y. (2014). Small interfering RNA directed against CTMP reduces acute traumatic brain injury in a mouse model by activating Akt. Neurol. Res. 36, 483–490.
60. Zhao, S., Fu, J., Liu, X., Wang, T., Zhang, J., and Zhao, Y. (2012). Activation of Akt/GSK–3beta/beta-catenin signaling pathway is in-

volved in survival of neurons after traumatic brain injury in rats. Neurol. Res. 34, 400–407.
61. Garling, R.J., Watts, L.T., Sprague, S., Fletcher, L., Jimenez, D.F., and Digicaylioglu, M. (2014). Does progesterone show neuroprotective effects on traumatic brain injury through increasing phosphorylation of Akt in the hippocampus? Neural Regen. Res. 9, 1891–1896.
62. Toker, A., and Marmiroli, S. (2014). Signaling specificity in the Akt pathway in biology and disease. Adv. Biol. Regul. 55, 28–38.
63. Padmaperuma, B., Mark, R., Dhillon, H.S., Mattson, M.P., and Prasad, M.R. (1996). Alterations in brain protein kinase C after experimental brain injury. Brain Res. 714, 19–26.
64. Lucke–Wold, B.P., Logsdon, A.F., Smith, K.E., Turner, R.C., Alkon, D.L., Tan, Z., Naser, Z.J., Knotts, C.M., Huber, J.D., and Rosen, C.L. (2015). Bryostatin-1 restores blood brain barrier integrity following blast-induced traumatic brain injury. Mol. Neurobiol. 52, 1119–1134.
65. Tan, Z., Turner, R.C., Leon, R.L., Li, X., Hongpaisan, J., Zheng, W., Logsdon, A.F., Naser, Z.J., Alkon, D.L., Rosen, C.L., and Huber, J.D. (2013). Bryostatin improves survival and reduces ischemic brain injury in aged rats after acute ischemic stroke. Stroke 44, 3490–3497.
66. Zohar, O., Lavy, R., Zi, X., Nelson, T.J., Hongpaisan, J., Pick, C.G., and Alkon, D.L. (2011). PKC activator therapeutic for mild traumatic brain injury in mice. Neurobiol. Dis. 41, 329–337.
67. Susarla, B.T., and Robinson, M.B. (2008). Internalization and degradation of the glutamate transporter GLT-1 in response to phorbol ester. Neurochem. Int. 52, 709–722.
68. Kobori, N., Moore, A.N., and Dash, P.K. (2015). Altered regulation of protein kinase a activity in the medial prefrontal cortex of normal and brain-injured animals actively engaged in a working memory task. J. Neurotrauma 32, 139–148.
69. Atkins, C.M., Chen, S., Alonso, O.F., Dietrich, W.D., and Hu, B.R. (2006). Activation of calcium/calmodulin-dependent protein kinases after traumatic brain injury. J. Cereb. Blood Flow Metab. 26, 1507–1518.
70. Underhill, S.M., and Wheeler, D.S. (2015). Differential regulation of two isoforms of the glial glutamate transporter EAAT2 by DLG1 and CaMKII. 35, 5260–5270.
71. Ubersax, J.A., and Ferrell, J.E., Jr. (2007). Mechanisms of specificity in protein phosphorylation. Nat. Rev. Mol. Cell Biol. 8, 530–541.
72. Pow, D.V., Naidoo, T., Lingwood, B.E., Healy, G.N., Williams, S.M., Sullivan, R.K., O'Driscoll, S., and Colditz, P.B. (2004). Loss of glial glutamate transporters and induction of neuronal expression of GLT-1B in the hypoxic neonatal pig brain. Brain Res. Dev. Brain Res. 153, 1–11.
73. Lin, C.L., Bristol, L.A., Jin, L., Dykes–Hoberg, M., Crawford, T., Clawson, L., and Rothstein, J.D. (1998). Aberrant RNA processing in a neurodegenerative disease: the cause for absent EAAT2, a glutamate transporter, in amyotrophic lateral sclerosis. Neuron 20, 589–602.

Address correspondence to:
Robert E. McCullumsmith, MD, PhD
Department of Psychiatry and Behavioral Neuroscience
University of Cincinnati
MSB 5255A
231 Albert Sabin Way
Cincinnati, OH 45267-0838

E-mail: robert.mccullumsmith@uc.edu